Hemin–Graphene Hybrid Nanosheets with Intrinsic Peroxidase-like Activity for Label-free Colorimetric Detection of Single-Nucleotide Polymorphism

Yujing Guo,[§,†,‡] Liu Deng,[§,†] Jing Li,[†] Shaojun Guo,[†] Erkang Wang,[†] and Shaojun Dong[†,*]

[†]State Key Laboratory of Electroanalytical Chemistry, Changchun Institute of Applied Chemistry, Chinese Academy of Sciences, Changchun 130022, Jilin, China and Graduate School of the Chinese Academy of Sciences, Beijing, 100039, P. R. China, and [‡]Research Center for Environmental Science and Engineering, Shanxi University, Taiyuan, 030006, China. [§] Yujing Guo and Liu Deng contributed equally to this work.

ABSTRACT This paper demonstrated for the first time a simple wet-chemical strategy for synthesizing hemin–graphene hybrid nanosheets (H-GNs) through the $\pi-\pi$ interactions. Significantly, this new material possesses the advantages of both hemin and graphene and exhibits three interesting properties. First, H-GNs have intrinsic peroxidase-like activity, which can catalyze the reaction of peroxidase substrate, due to the existence of hemin on the graphene surface. Second, their dispersion follow the 2D Schulze–Hardy rule, that is to say, the coagulation of H-GNs in electrolyte solution results from the interplay between van der Waals attraction and electric double-layer repulsion. Third, H-GNs exhibit the ability to differentiate ss- and ds-DNA in optimum electrolyte concentration, owing to the different affinities of ss- and ds-DNA to the H-GNs. On the basis of these unique properties of the as-prepared H-GNs, we have developed a label-free colorimetric detection system for single-nucleotide polymorphisms (SNPs) in disease-associated DNA. To our knowledge, this is the first report concerning on SNPs detection using functionalized graphene nanosheets. Owing to its easy operation and high specificity, it was expected that the proposed procedure might hold great promise in the pathogenic diagnosis and genetic diseases.

KEYWORDS: graphene nanosheet · hemin · single-nucleotide polymorphism · artificial enzyme mimetic

Graphene, a novel one-atom-thick two-dimensional graphitic carbon system, has recently emerged as a fascinating material. Owing to its large specific surface area, high thermal and electrical conductivities, great mechanical strength, and low manufacturing cost, the study on graphene has attracted considerable attention from both the experimental and theoretical scientific communities.[1,2] Its unique nanostructure holds great promise for various applications including nanoelectronics, nanophotonics, field effect transistors, energy and storage devices, nanocomposites, sensors, and catalysis, *etc*.[3–5] Using graphene oxides (GO) as the starting material to produce graphene has turned out to be an efficient and economic process for mass production.[6] At the same time, this procedure can provide graphene with processability and new functions. Noncovalent functionalization is of great interest for the solubility of graphene, because this strategy enables the attachment of molecules through $\pi-\pi$ stacking and hydrophobic interactions while still preserving the intrinsic properties of graphene.[7] However, multifunctional materials, formed by the noncovalent attachment taking advantage of both the superior properties of graphene and the functionalizing molecules, have not been adequately explored.[8]

Hemin (iron protoporphyrin) is the active center of heme-proteins, such as cytochromes, peroxidase, myoglobin, and hemoglobin, which has the peroxidase-like activity similar to the peroxidase enzyme.[9] It also possesses a large extinction coefficient in the visible-light region, predictable rigid structures, and prospective photochemical electron-transfer ability. The deposition of porphyrin on the graphene oxide sheets through $\pi-\pi$ interaction was successfully realized.[10,11] If we can obtain the hemin–graphene hybrid nanosheets, it will provide excellent opportunities for applications in the fields of artificial enzyme mimetics, biosensors, electrocatalysis, luminescence, and electronics, *etc*.

Human genome mutations are the key factors in genetic disorders, predisposition to diseases, and discrepancies in the response to drugs and therapeutics.[12] In human genome, the most prevalent and stably inherited types of sequence variations are the single-nucleotide polymorphisms (SNPs). Studies have shown the close associations between SNPs and tumor development or progression and the analysis of SNPs can provide a tool for early diagnosis and risk assessment of malignancy.[13]

*Address correspondence to dongsj@ciac.jl.cn.

Received for review November 2, 2010 and accepted December 27, 2010.

Published online January 10, 2011
10.1021/nn1029586

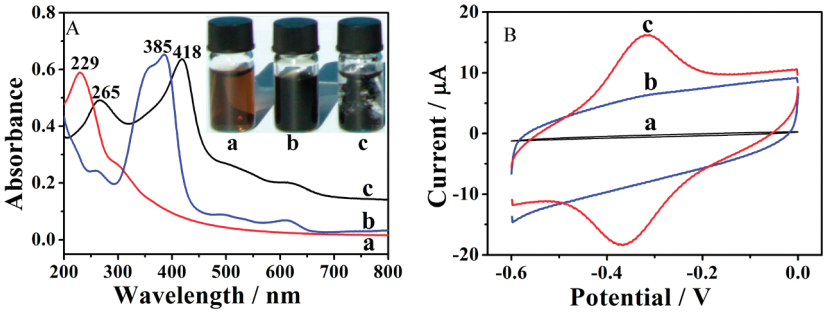

Figure 1. (A) UV−visible spectra of GO suspension (a), hemin solution (b), H-GNs suspension (c). Inset: photographs of GO (a), H-GNs (b), and GNs (c) dispersion in water. (B) Cyclic voltammograms of bare GCE (a), GNs/GCE (b), and H-GNs/GCE in 0.1 M PBS (pH 7.4) saturated with N_2 at a scan rate of 0.05 V s^{-1}.

Therefore, developing convenient and sensitive methods for the detection of SNPs have gained much attention, with the hope of rapid and reliable genetic analysis of diseases and subtle genetic risk factors.[14,15] Conventional methods involved allele-specific DNA hybridization,[16] ligation, or primer extension,[17] molecular-beacon-based fluorescence resonance energy transfer,[18−20] electrochemical typing,[21,22] and binary DNA probe-assisted assays,[23] provide accurate validation but have disadvantages either using complex procedures or the employment of expensive instrument.[24] The idea that a nucleotide change could be directly detected by the naked eye without the aid of equipments is attractive. The nanomaterial probes (*e.g.*, gold nanoparticles, carbon nanotubes) were widely applied as the sensing element to detect DNA in colorimetric assay.[25−27] The DNAzyme and single wall carbon nanotubes were applied as the artificial peroxidase, which can catalyze 3,3′,5,5′-tetramethylbenzidine (TMB) or 2,2′-azinobis(3-ethylbenzothiozoline)-6-sulfonic acid (ABTS) into color solution to determinate DNA.[28−30] Therefore, synthesis of new materials which possess both peroxidase activity and DNA identify ability is very attractive in DNA assay. Previous studies reported that graphene oxide (GO) was able to differentiate single-stranded DNA (ss-DNA) and double-stranded DNA (ds-DNA), owing to the different affinities of ss- and ds-DNA on it.[31,32] So that, how to obtain the graphene with peroxidase activity while possessing the intrinsic discrimination ability of ss- and ds-DNA is quite challenging.

In this paper, hemin−graphene hybrid nanosheets (H-GNs) were synthesized by simple wet-chemical strategy through the $\pi-\pi$ interaction. Significantly, the new nanocomposite possesses both excellent properties of graphene and hemin. H-GNs not only have the intrinsic peroxidase-like activity of hemin that can catalyze the reaction of peroxidase substrate in the presence of H_2O_2, but also possess the ability of graphene to distinguish ss- and ds-DNA. On the basis of this novel material, we have developed a label-free colorimetric detection system for SNPs in Hepatitis B virus (HBV) for the first time. This H-GNs based label-free colorimetric method may be useful in clinical diagnosis of genetic diseases that contain single nucleotide mutations. Furthermore, in comparison to other nanomaterials, the environment friendly, cost efficient and large production scale of H-GNs makes it a promising material for biotechnology, biosensors, and medicine, *etc.*

RESULTS AND DISCUSSION

Formation of Hemin-Functionalized Graphene Nanosheets. As shown in Figure 1A, the GO dispersion displays a maximum absorption at 231 nm which is due to the $\pi-\pi^*$ transition of aromatic C═C bonds and a shoulder at *ca.* 290−300 nm which corresponds to the n−π^* transition of the C═O bond.[33] The spectrum of hemin solution contains a strong peak at 385 nm attributed to the Soret band, as well as a group of weak peaks between 500 and 700 nm ascribed to the Q-bands. After reduction, the color of the GO dispersion changes from pale-yellow (Figure 1A, inset a) to black (Figure 1A, inset b). The H-GNs exhibit a broad absorption at 265 nm which should be the corresponding reduced graphene oxide. An absorption at 418 nm is also observed, which corresponds to the Soret band of hemin with a large bathochromic shift (33 nm). These findings indicate the existence of the $\pi-\pi$ interactions between GO and hemin, which are in good agreement with the previous report that interactions of a cationic porphyrin derivative with chemical converted graphene result in a red shift of the porphyrin Soret band.[34] This clearly confirms that hemin molecules are attached to GNs. Particularly, the dispersion is stable and no obvious precipitates are observed after being stored for more than 6 months (Figure 1A, inset b). In contrast, the reduction of GO dispersion without any stabilizer led to the precipitation of GNs after being stored for less than 2 weeks (Figure 1A, inset c), due to their irreversible aggregation.

The attachment of hemin on graphene surface was also characterized by electrochemical method. Figure 1B shows cyclic voltammograms recorded at the bare glassy carbon electrode (GCE) (a), the graphene nanosheets modified GCE (GNs/GCE) (b), and the H-GNs modified GCE (H-GNs/GCE) (c) in N_2-saturated phosphate

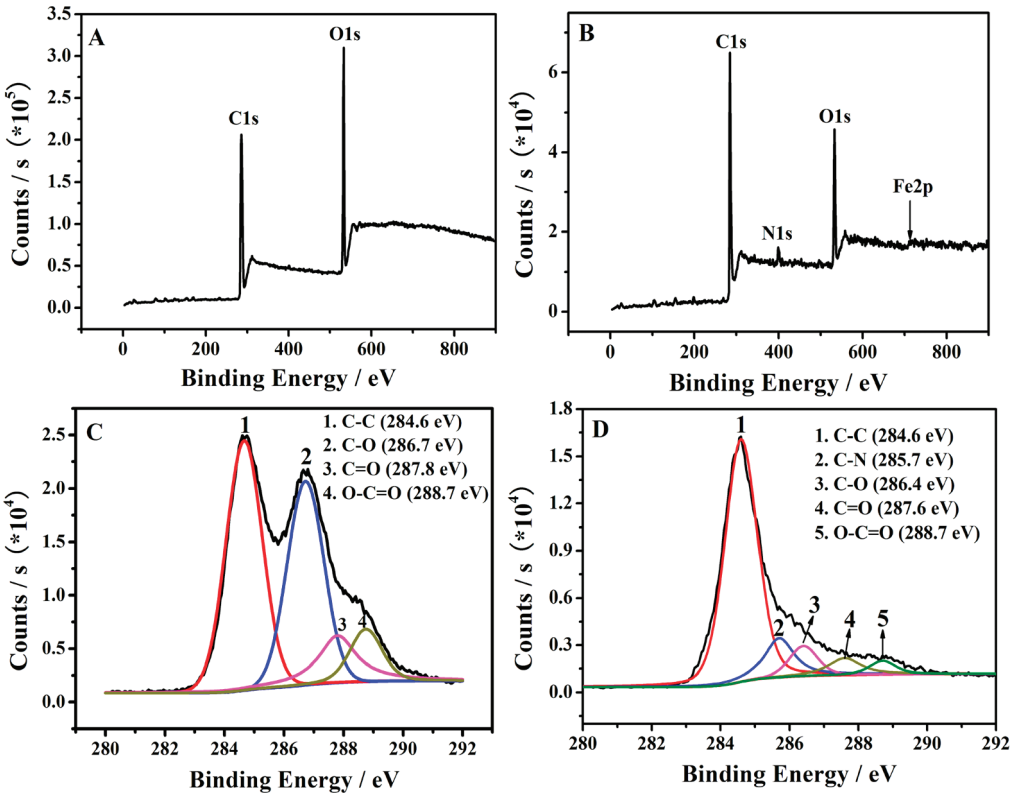

Figure 2. Survey XPS data for GO (A) and H-GNs (B). The deconvolution of C1s spectra of GO (C) and H-GNs (D).

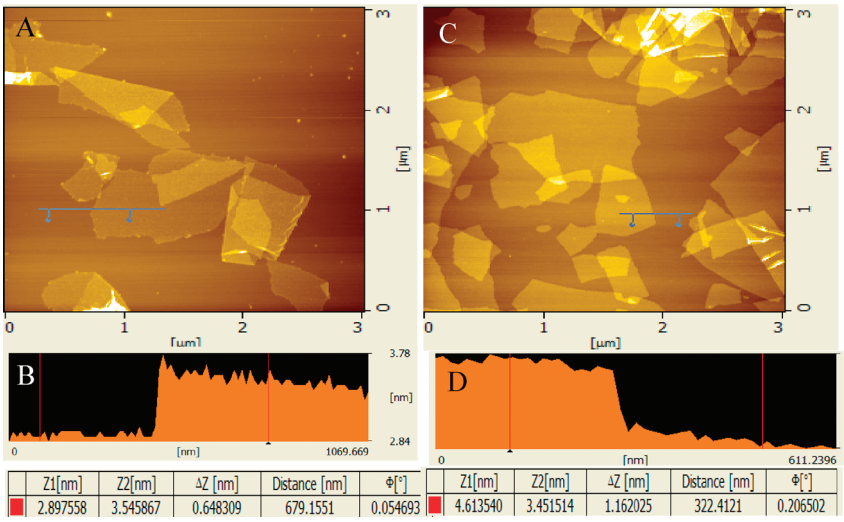

Figure 3. AFM images of GNs (A) and H-GNs (C). The cross section identified by the line shows the heights of GNs (B) and H-GNs (D).

buffer solution (PBS). As expected, in the absence of H-GNs, no redox peaks were observed for either electrode in the potential range investigated. By contrast, a pair of well-defined redox peaks were clearly seen when the H-GNs were presented on the electrode surface. The formal potential ($E^{o\prime}$) was estimated as −0.34 V (*vs* Ag/AgCl in saturated KCl) with the peak-to-peak separation of 56 mV and equal cathodic to anodic current intensity. The redox peaks should be ascribed only to hemin, which is the characteristic of a single electron transfer process of iron at the core of hemin for the $\text{hemin}_{ox}/\text{hemin}_{red}$ pair.[35]

X-ray photoelectron spectroscopy (XPS) was employed to further explore the interactions between GO and hemin. The survey (Figure 2A) of GO showed the absence of any detectable amounts Fe2p at about 712 eV and N1s at about 400 eV. Compared with GO, the survey of H-GNs (Figure 2B) showed the presence of N1s and Fe2p originating from hemin, indicating that the noncovalent functionalization of graphene by hemin successfully occurred. The deconvolution of C1s spectrum of GO (Figure 2C) indicated the presence of four types of carbon bonds: C−C (284.6 eV), C−O (286.7 eV),

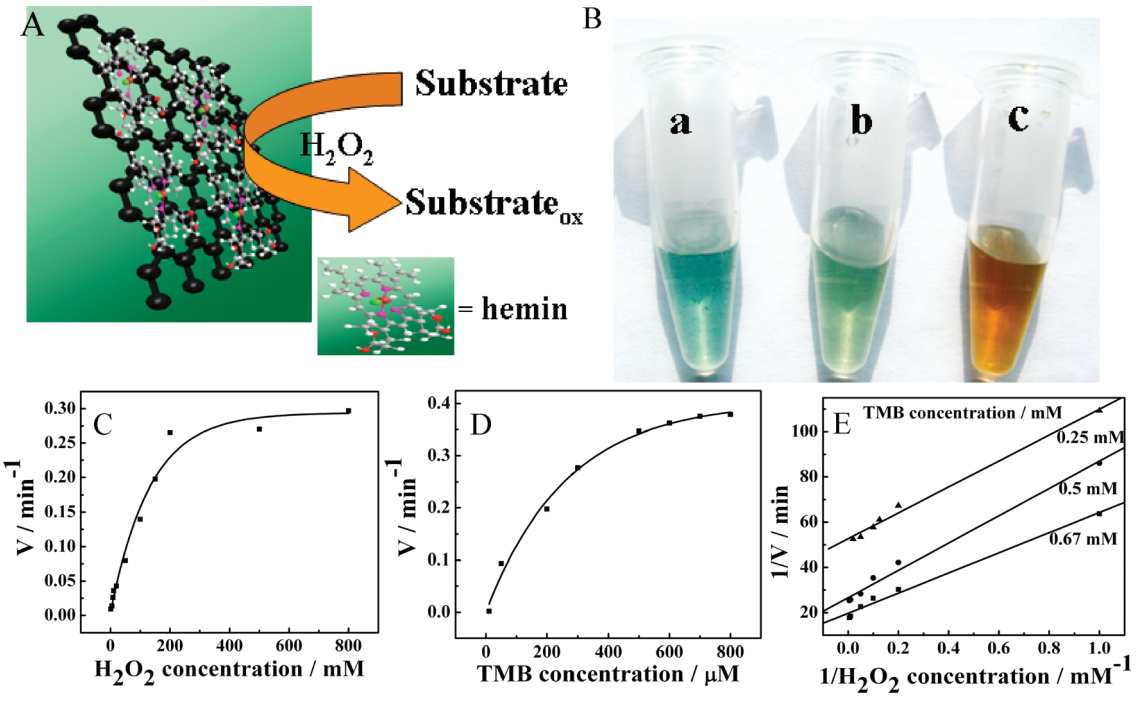

Figure 4. (A) Schematic illustration of peroxidase-like activity of H-GNs. (B) The H-GNs catalyze oxidation of various peroxidase substrates in the presence of H_2O_2 to produce different color reactions. (a) TMB; (b) ABTS; (c) OPD. (C, D, E) Steady-state kinetic assay and catalytic mechanism of H-GNs. (C, D) The velocity (*v*) of the reaction was measured using 1 μg H-GNs in 1 mL of 25 mM PBS (pH 5.0) at room temparature. (C) The concentration of TMB was 0.8 mM and the H_2O_2 concentration was varied. (D) The concentration of H_2O_2 was 10 mM and the TMB concentration was varied. (E) Double-reciprocal plots of activity of H-GNs at a fixed concentration of one substrate *versus* varying concentration of the second substrate for H_2O_2 and TMB. The *y*-axis values are observed absorbance values.

C═O (287.8 eV), and O−C═O (288.7 eV). After its reduction, the peaks associated with C−C or C−H (284.6 eV) became predominant, while the peaks related to the oxidized carbon species were greatly weakened (Figure 2D). These results further indicate that GO has been well deoxygenated to form H-GNs. Meanwhile, a new peak corresponding to C−N species, which results from the bond formation by hydrazine, appears at 285.7 eV in the spectra of H-GNs corresponding to the carbon in the C−N bonds.[36] These results indicate that the reduced GNs were protected by hemin molecules.

The morphology and thickness of H-GNs have been studied by AFM observation. The thickness of the graphene sheets is about 0.65 nm (Figure 3A,B). It was comparable with that of the typical single-layer exfoliated sheets prepared by the annealing method in ultrahigh vacuum (0.6 nm).[37] The average thickness of H-GNs is determined to be about 1.16 nm (Figure 3C,D). There was 0.51-nm increment compared with that of unmodified graphene, owing to the presence of hemin on the graphene sheet surfaces. Since hemin could locate on both sides of the graphene, the thickness of hemin layer on graphene was calculated to be about 0.25 nm. This data was consistent with the thickness of a single hemin molecule (0.2 nm).[38] So we assumed that graphene nanosheets were covered by a monolayer of hemin. The coverage of hemin on graphene is calculated to be about 20.22% by comparing the absorbance of H-GNs and hemin.

TABLE 1. Comparison of the Kinetic Parameters of H-GNs and HRP[a]

	substrate	K_m (mM)	V_{max} (M s^{-1})
H-GNs	TMB	5.100	4.55×10^{-8}
H-GNs	H_2O_2	2.256	5.06×10^{-8}
HRP	TMB[39]	0.434	10.00×10^{-8}
HRP	H_2O_2[39]	3.70	8.71×10^{-8}
hemin	TMB	4.84	4.69×10^{-8}
hemin	H_2O_2	2.74	3.53×10^{-8}

[a] K_m is the Michaelis constant; V_{max} is the maximal reaction velocity.

Peroxidase-like Activity of H-GNs. As we know, hemin is the activate site in peroxidase enzyme and exhibits the peroxidase-like activity similar to the peroxidase enzyme.[9] So that H-GNs are expected to show the peroxidase-like activity as illustrated in Figure 4A. Figure 4B shows the H-GNs catalyzed oxidation reaction of different peroxidase substrates such as TMB, ABTS, and o-phenylenediamine (OPD) in the presence of H_2O_2 to give the same color changes as HRP. To investigate the roles of hemin and graphene in peroxidase-like activity of H-GNs, we compared the activity of hemin and graphene with that of H-GNs under the same condition. As shown in Supporting Information, Figure S1, graphene exhibited much less activity than

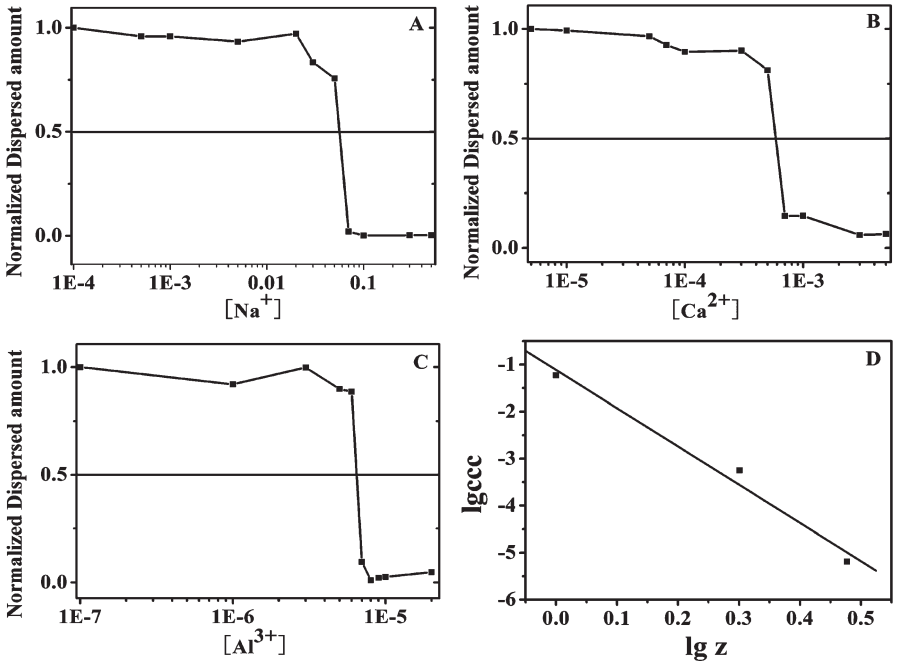

Figure 5. Normalized concentrations of H-GNs against NaCl (A), $CaCl_2$ (B), and $AlCl_3$ (C) concentrations. (D) Double logarithmic plot of the critical coagulation concentrations against the ionic valency. The solid line has a slope of *ca.* −9.

H-GNs or hemin, showing that the observed peroxidase-like activity is attributed to hemin on the graphene surface. The optimal pH was approximately 5.0 (Supporting Information, Figure S2), which was very similar to the value of hemin, and also confirmed the key factor of hemin in H-GNs. To characterize the peroxidase-like activity of H-GNs, the typical Michaelis−Menten curves were shown in Figure 4C,D, which were in accordance with hemin (Supporting Information, Figure S3). With the Lineweaver−Burk equation, the Michaelis constant (K_m) and the maximal reaction velocity (V_{max}) were obtained and shown in Table 1. The apparent K_m value of H-GNs was similar with hemin, which further confirmed that H-GNs retained the peroxidase activity of hemin. The apparent K_m value of the H-GNs with TMB as the substrate was significantly higher than that for HRP (Table 1). The apparent K_m value of the H-GNs with H_2O_2 as the substrate was lower than HRP (Table 1), suggesting that the H-GNs have a higher affinity for H_2O_2 than HRP. To further investigate the mechanism of H-GNs catalysis, we measured their activity over a range of TMB and H_2O_2 concentrations. The double reciprocal plots of initial velocity against the concentration of one substrate are obtained over a range of concentrations of the second substrate (Figure 4E). These parallel lines are the characteristic of a ping-pong mechanism, as observed for peroxidase enzyme (HRP).[39] Taken together, these results demonstrate that H-GNs retained intrinsic peroxidase-like activity as the same as hemin. Compared to the peroxidase enzyme, the inorganic H-GNs make them suitable for a broad range of applications in the biomedicine and environmental chemistry fields.

TABLE 2. Critical Coagulation Concentrations (ccc) for Various Ions

ions	Na^+	Ca^{2+}	Al^{3+}
ccc (mM)	58	0.56	0.0065

Solubility of H-GNs in Ionic Conditions. To investigate whether H-GNs are able to discriminate ss- and ds-DNA as the graphene oxide, the aggregation behavior of H-GNs in salt solution was studied first. The as prepared H-GNs can disperse well in water; however, we found that the high salt concentration could induce them to coagulate. It is well-known that the critical coagulation concentration (ccc), the minimum concentration of ions necessary to cause rapid coagulation of colloids, followed the Schulze-Hardy rule:[40]

$$\log(\mathrm{ccc}) \approx n \log\left(\frac{1}{z}\right) \quad (1)$$

where z is the valency of the electrolyte counterions. Typically, n is 6 in three dimensions (3D) and 9 in two dimensions (2D). For the first time, the coagulation behavior of graphene in different electrolytes solution was studied. All the electrolytes are supplied as chloride salts in the form of XCl_z, where X is Na^+, Ca^{2+} or Al^{3+}. Figure 5A displayed the coagulation curve for H-GNs in water as a function of NaCl concentration. The concentration of H-GNs *versus* NaCl concentration is constant until it abruptly decreases with the NaCl concentration exceeding a threshold value. When the normalized H-GNs concentration became 0.5, this NaCl concentration is considered as the ccc of Na^+ for H-GNs. Coagulation curve for Ca^{2+} and Al^{3+} ions were

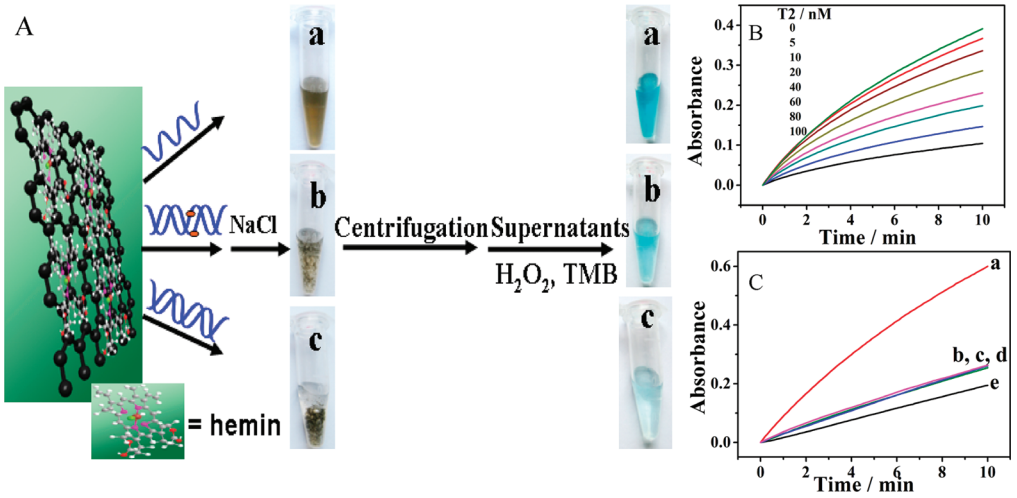

Figure 6. (A) Protocol for SNPs detection. (a) ssDNA (T1) (no precipitation, dark blue), (b) single mismatched duplex DNA (T2/T3) (small amount of precipitation, blue), and complementary duplex DNA (T1/T2) (much precipitation, light blue). (B) Time-dependent absorbance changes at 652 nm in the presence of different amounts of T2 with the fixed concentration of T1(100 nM). (C) Time-dependent absorbance changes at 652 nm with corresponding supernatant in (a) ssDNA (T1); (b, c, d) single mismatched duplex DNA (T2/T3 or T4, T5); (e) complementary duplex DNA (T1/T2) in PBS at room temperature. The concentration of TMB is 0.8 mM and that of H_2O_2 is 10 mM.

shown in Figure 5B,C, and the obtained ccc values for all ions were summarized in Table 2. The double-logarithmically plot of ccc for different ions against the ionic valence was shown in Figure 5D. The slope of this line was ~8.13 which was close to 9, that is to say, H-GNs dispersion followed the 2D Schulze−Hardy rule. The fact that H-GNs followed the Schulze−Hardy rule gives us deep insight into the interactions between H-GNs. According to the Derjaguin−Landau−Verwey−Overbeek (DLVO) theory, the Schulze−Hardy rule results from interplay between van der Waals attraction and electric double-layer repulsion. Therefore we can conclude that the suspension of H-GNs will coagulate once the concentration of inorganic electrolyte in the medium exceeds the ccc owing to the charge screening effects.

Sensor Applications. To verify the as prepared H-GNs having different affinities toward ss- and ds-DNA as the graphene oxide, the ss- and ds-DNA were added to H-GNs solution with 0.6 M Na^+. From Supporting Information, Figure S4, it was found that the ss-DNA/H-GNs were well suspended in the medium, while the coagulation of ds-DNA/H-GNs was observed visually. In the previous report,[31] ssDNA can stably be adsorbed by the graphene oxide, due to the $\pi-\pi$ stacking interaction between the ring structure in the nucleobases and the hexagonal cells of the graphene oxide. Since the prepared H-GNs have rigid planar construction and big unlocalized π bond, ssDNA should adsorb stably on to H-GNs surface by the same interaction. It was found that much higher concentration of Na^+ is required to make H-GNs coagulate completely in the presence of ssDNA, since the negatively charged DNA backbone on H-GNs surface increases individual H-GNs electrostatic repulsion and resists salt-induced H-GNs aggregation. In contrast, dsDNA cannot stably adsorb on H-GNs and retain its helical structure because the ring structure of nucleobases was effectively shielded within the densely negatively charged phosphate backbone of dsDNA. So at the optimum ion concentratiom, the H-GNs can distinguish ss- and ds-DNA.

By combining the peroxidase activity and ss-, ds-DNA differentiate ability of H-GNs, we developed a label-free colorimetric detection method for DNA sequence specificity on the basis of H-GNs as a peroxidase and identify element. The protocol of our method is displayed in Figure 6A. H-GNs solution with dsDNA was easily precipitated by adding electrolyte, whereas H-GNs with ssDNA could inhibit precipitation. In the presence of TMB and H_2O_2, the H-GNs supernatant will catalyze a color reaction that can be judged by the naked eye and easily be monitored by the absorbance changes at 652 nm. Figure 6B showed time-dependent absorbance changes in the presence of different amounts of 29 mer HBV DNA. It was found that the absorbance of the centrifugal supernatants decrease linearly with the concentration of complementary target DNA in the range of 5−100 nM with a limit of detection around 2 nM, comparable to previously reported systems based on MWNT light scattering,[27] SWNT intrinsic peroxidase activity, or GO fluorescence quenching.[28,31] More importantly, this DNA sensor was of sufficient selectivity to easily differentiate single mismatches, which offered the opportunity to determinate SNPs. We attempted to detect the mutation in the HBV gene; the retroviruses randomly generate mutations during their rapid multiplication process, which leads to resistance against antiviral drugs. As shown in Figure 6C, the absorbance change for the single mismatched duplex DNA (T3−T5, either "A", "T" or "C") was approximately three times higher than that

for complementary duplex DNA (T1/T2). As the concentration of T2 and T3 increased from 20 to 200 nM, the color difference could be distinguished even by the naked eye (Figure 6A-b,c). This high sequence specificity for single mismatches was quite impressive, indicating that this method is sensitive and can detect SNPs in human DNA. Because of the higher catalytic activity of H-GNs, the amount of H-GNs used in our paper for colorimetric DNA detection was 1 μg/mL while that of SWNT used in previous report was 20 μg/mL.[28] This much lower amount would reduce the reagent consumption in real sample detection, which is important in medical industry. Compared to the expensive price of SWNT, the simple, cheap method of the H-GNs preparation will facilitate practical application. The intrinsic peroxidase-like activity of H-GNs and the ability to differentiate ss- and dsDNA not only offer a new approach to detect SNPs, but also may find potential applications in detecting a wide range of analytes with the use of functional nucleic acid structure.

CONCLUSIONS

Hemin−graphene hybrid nanosheets have been successfully prepared by a simple wet-chemical strategy. This new nanomaterial exhibits high solubility and stability in water. Significantly, H-GNs have the advantages of both hemin and graphene. They possess intrinsic peroxidase-like activity attributed to the presence of hemin. Also, they are able to differentiate ss- and ds-DNA in optimum salt concentration owing to the different affinities of ss- and ds-DNA to graphene. On the basis of these unique properties of the new material, we developed a novel assay for SNPs detection. This assay is simple, rapid, cost-efficient, and there is no need to label DNA substrate. The most important characteristic of the assay is as sensitive probe for direct visualization of SNPs by the naked eye at room temperature, which makes it more convenient than other methods that rely on complex instrumentation.

EXPERIMENTAL SECTION

Materials. DNA oligonucleotides were purchased from Sangon, Inc. (Shanghai, China), and were used as received: wild-type HBV DNA (T1), 5′-TTGTCCTGGCTATCGCTGGATGTGTCTGC-3′; fully complementary oligomer (T2), 5′-GCAGACACATCCAGC-GATAGCCAGGACAA-3′; single mismatch mutated HBV DNA (T3), 5′-TTGTCCTGGCTATCTCTGGATGTGTCTGC-3′; single mismatch mutated HBV DNA (T4), 5′- TTGTCCTGGCTATCACTG-GATGTGTCTGC-3′; single mismatch muntated HBV DNA (T5), 5′-TTGTCCTGGCTATCCCTGGATGTGTCTGC-3′; graphite was purchased from Alfa Aesar. Hemin, 2,2′-azinobis(3-ethylbenzothiozoline)-6-sulfonic acid (ABTS), and 3,3′,5,5′-tetramethylbenzidine (TMB) were obtained from Sigma. *o*-Phenylenediamine (OPD) and hydrazine solution (50%) was purchased from Shanghai Chemical Plant, (Shanghai, China). Other chemicals were of analytical grade and used without further purification. Water used throughout all experiments was purified with the Millipore system.

Apparatus. TEM images were obtained with a JEM-2100F high-resolution transmission electron microscope operating at 200 kV. AFM image was taken by using a SPI3800N microscope (Seiko Instruments Industry Co., Tokyo, Japan) (Seiko Instruments, Inc.) operating in the tapping mode with standard silicon nitride tips. Typically, the surface was scanned at 1 Hz with the resolution of 256 lines/image. The XPS measurement was performed on an ESCALAB-MKII 250 photoelectron spectrometer (VG Co.) with Al Kα X-ray radiation as the X-ray source for excitation. UV−vis absorption spectra were recorded on a Cary 500 UV−vis spectrophotometer (Varian, U.S.A.). Electrochemical measurements were carried out on CHI832B electrochemical workstation (ChenHua Instruments Co., Shanghai, China). A three-electrode system was used in the experiment with a bare and the modified glassy carbon electrode (3 mm in diameter) as the working electrode, respectively. An Ag/AgCl electrode (saturated KCl) and a Pt wire electrode were used as reference and counter-electrode, respectively.

Synthesis of Hemin Functionalized Graphene Nanosheets and Pure Graphene. GO nanosheets were synthesized from natural graphite by Hummers' method with little modification.[41−43] H-GNs were prepared as followed: 20.0 mL of the homogeneous graphene oxide dispersion (0.5 mg/mL) was mixed with 20.0 mL of 0.5 mg/mL hemin aqueous solution and 200.0 μL of ammonia solution, followed by the addition of 30 μL of hydrazine solution. After being vigorously shaken or stirred for a few minutes, the vial was put in a water bath (60 °C) for 3.5 h. The stable black dispersion was obtained. The dispersion was filtered with a nylon membrane (0.22 μm) to obtain H-GNs that can be redispersed readily in water by ultrasonication. Additionally, the preparation of pure graphene was similar to H-GNs except no addition of hemin.

Preparation of Graphene and Hemin-Graphene Modified Electrode. Prior to modification, the glassy carbon electrode (GCE, 3 mm) was polished with 1, 0.3, and 0.05 μm alumina slurry, rinsed thoroughly with doubly distilled water between each polishing step, then washed successively with 1:1 nitric acid, acetone, and doubly distilled water in an ultrasonic bath and dried in air. The graphene-nanosheets-modified GCE (GNs/GCE) and the H-GNs-modified GCE (H-GNs/GCE) were obtained by casting 5 μL of 0.25 mg/mL GNs or H-GNs suspension on the surface of well-polished GCE, which were dried in air. Finally, the modified electrodes were activated by several successive scans with a scan rate of 50 mV/s in phosphate buffer solution (pH 7.4) until a steady voltammogram was obtained.

Determination of Critical Coagulation Concentration (ccc). A 70 μL portion of 0.25 mg/mL H-GNs were added to 930 μL of different concentrations of standard electrolytes solution, respectively. All electrolytes are supplied as chloride salts in the form of XClz, where X = Na^+, Ca^{2+}, or Al^{3+}. The dispersions were left undisturbed for 5 h at room temperature. Then they were centrifuged at 3000 rpm for 1 min, and the concentration of H-GNs in the supernatant solution was determined by measuring the absorbance.

Kinetic Analysis. Steady state kinetic assays were carried out at room temperature with 1 μg H-GNs in 1 mL of 25 mM phosphate buffer solution (pH 5.0) in the presence of 10 mM H_2O_2, using 0.8 mM TMB as the substrate, unless otherwise stated.

All the reactions were monitored in timescan mode at 652 nm using a Cary 500 UV−vis spectrophotometer. The apparent kinetic parameters were calculated based on the function $\nu = V_{max}C/(K_m + C)$ where ν is the initial velocity, V_{max} is the maximal reaction velocity, C is the concentration of the substrate, and K_m is the Michaelis−Menten constant.[40]

To investigate the mechanism, assays were carried out under standard reaction conditions as described above by varying concentrations of TMB at a fixed concentration of H_2O_2 or *vice versa*.

Bioassay. Hybridization of ssDNA (T1, 50 μL 2 μM) with different concentrations of its complementary target DNA (T2) were conducted at 95 °C in buffer (25 mM Tris-HAc buffer

solution, pH 7.4), and the mixtures were cooled to room temperature. Then 10 μL of the above hybridization solution was added to 190 μL of 1 μg/mL H-GNs solution, respectively, and incubated for 2 min. After that NaCl was added to the above solution to a final concentration of 0.6 M. The solution stood for 60 min at room temperature and then was diluted to 1 mL before being centrifuged at 3000 rpm for 1 min. Then 250 μL of the supernatant was added to 750 μL of PBS (pH 5.0). After that TMB and H_2O_2 were added to final concentrations of 0.8 mM and 10 mM, respectively. The time-course measurements were done at the Cary 500 UV−vis−NIR spectrometer. SNPs detection was performed according to the above procedure on hybridization of different concentrations of T3 (or T4, T5) with T2.

Acknowledgment. This work was supported by the National Natural Science Foundation of China (Nos. 20675076, 20735003 and 20820102037), the 973 Project (Nos. 2009CB930100 and 2010CB933600) and the China Postdoctoral Science Foundation (No. 20090451143).

Supporting Information Available: Typical absorption curves of TMB catalytically oxidized by G; H-G and hemin in the presence of H_2O_2; the effect of pH on the peroxidase-like activity of hemin and H-GNs; steady-state kinetic assay and catalytic mechanism of hemin; photographs of H-GNs in NaCl soulution in the absence and presence of ssDNA and dsDNA. This material is available free of charge *via* the Internet at http://pubs.acs.org.

REFERENCES AND NOTES

1. Rao, C. N. R.; Sood, A. K.; Subrahmanyam, K. S.; Govindaraj, A. Graphene: The New Two-Dimensional Nanomaterial. *Angew. Chem., Int. Ed.* **2009,** *48*, 7752–7777.
2. Xu, Y. X.; Bai, H.; Lu, G. W.; Li, C.; Shi, G. Q. Flexible Graphene Films *via* the Filtration of Water-Soluble Noncovalent Functionalized Graphene Sheets. *J. Am. Chem. Soc.* **2008,** *130*, 5856–1857.
3. Guo, S. J.; Dong, S. J. Graphene Nanosheet: Synthesis, Molecular Engineering, Thin Film, Hybrids, and Energy and Analytical Applications, *Chem. Soc. Rev.* 2010, DOI:10.1039/C0CS00079E.
4. Guo, S. J.; Dong, S. J.; Wang, E. K. Three-Dimensional Pt-on-Pd Bimetallic Nanodendrites Supported on Graphene Nanosheet: Facile Synthesis and Used as an Advanced Nanoelectrocatalyst for Methanol Oxidation. *ACS Nano* **2010,** *4*, 547–555.
5. Guo, S. J.; Wen, D.; Dong, S. J.; Wang, E. K. Platinum Nanoparticle Ensemble-on-Graphene Hybrid Nanosheet: A New Electrode Material for Electrochemical Sensing. *ACS Nano* **2010,** *4*, 3959–3968.
6. Eda, G.; Fanchini, G.; Chhowalla, M. Large-Area Ultrathin Films of Reduced Graphene Oxide as a Transparent and Flexible Electronic Material. *Nat. Nanotechnol.* **2008,** *3*, 270–274.
7. Su, Q.; Pang, S.; Alijani, V.; Li, C.; Feng, X.; Müllen, K. Composites of Graphene with Large Aromatic Molecules. *Adv. Mater.* **2009,** *21*, 3191–3195.
8. Ghosh, A.; Rao, K. V.; George, S. J.; Rao, C. N. R. Noncovalent Functionalization, Exfoliation, and Solubilization of Graphene in Water by Employing a Fluorescent Coronene Carboxylate. *Chem.—Eur. J.* **2010,** *16*, 2700–2704.
9. Zhang, G.; P. Dasgupta, K. Hematin as a Peroxidase Substitute in Hydrogen Peroxide Determinations. *Anal. Chem.* **1992,** *64*, 517–522.
10. Xu, Y.; Liu, Z.; Zhang, X.; Wang, Y.; Tian, J.; Huang, Y.; Ma, Y.; Zhang, X.; Chen., Y. A Graphene Hybrid Material Covalently Functionalized with Porphyrin: Synthesis and Optical Limiting Property. *Adv. Mater.* **2009,** *21*, 1275–1279.
11. Geng, J.; Jung, H.-T. Porphyrin Functionalized Graphene Sheets in Aqueous Suspensions: from the Preparation of Graphene Sheets to Highly Conductive Graphene Films. *J. Phys. Chem. C* **2010,** *114*, 8227–8234.
12. Altshuler, D.; Brooks, L. D.; Chakravarti, A.; Collins, F. S.; Daly, M. J.; Donnelly, P. A Haplotype Map of the Human Genome. *Nature* **2005,** *437*, 1299–1320.
13. McCarthy, J. J.; Hilfiker, R. The Use of Single-Nucleotide Polymorphism Maps in Pharmacogenomics. *Nat. Biotechnol.* **2000,** *18*, 505–508.
14. Wan, Y.; Lao, R.; Liu, G.; Song, S.; Wang, L.; Li, D.; Fan, C. Multiplexed Electrochemical DNA Sensor for Single-Nucleotide Polymorphism Typing by Using Oligonucleotide-Incorporated Nonfouling Surfaces. *J. Phys. Chem. B* **2010,** *114*, 6703–6706.
15. Kato, D.; Sekioka, N.; Ueda, A.; Kurita, R.; Hirono, S.; Suzuki, K.; Niwa, O. Nanohybrid Carbon Film for Electrochemical Detection of SNPs without Hybridization or Labeling. *Angew. Chem., Int. Ed.* **2008,** *47*, 6681–6684.
16. Wallace, R. B.; Shaffer, J.; Murphy, R. F.; Bonner, J.; Hirose, T.; Itakura, K. Hybridization of Synthetic Oligodeoxyribonucleotides to φX 174 DNA: the Effect of Single Base Pair Mismatch. *Nucleic Acids Res.* **1979,** *6*, 3543–3558.
17. Hagenbuch, P.; Kervio, E.; Hochgesand, A.; Plutowski, U.; Richert, C. Chemical Primer Extension: Efficiently Determining Single Nucleotides in DNA. *Angew. Chem., Int. Ed.* **2005,** *44*, 6588–6592.
18. Tyagi, S.; Kramer, F. R. Molecular Beacons: Probes that Fluoresce upon Hybridization. *Nat. Biotechnol.* **1996,** *14*, 303–308.
19. Wang, K.; Tang, Z.; Yang, C. J.; Kim, Y.; Fang, X.; Li, W.; Wu, Y.; Medley, C. D.; Cao, Z.; Li, J.; Colon, P.; Lin, H.; Tan, W. Molecular Engineering of DNA: Molecular Beacons. *Angew. Chem., Int. Ed.* **2009,** *48*, 856–870.
20. Xiao, Y.; Plakos, K. J. I.; Lou, X.; White, R. J.; Qian, J.; Plaxco, K. W.; Soh, H. T. Fluorescence Detection of Single-Nucleotide Polymorphisms with a Single, Self-Complementary, Triple-Stem DNA Probe. *Angew. Chem., Int. Ed.* **2009,** *48*, 4354–4358.
21. Liu, G.; Wan, Y.; Gau, V.; Zhang, J.; Wang, L.; Song, S.; Fan, C. An Enzyme-Based E-DNA Sensor for Sequence-Specific Detection of Femtomolar DNA Targets. *J. Am. Chem. Soc.* **2008,** *130*, 6820–6825.
22. Huang, Y.; Zhang, Y.; Xu, X.; Jiang, J.; Shen, G.; Yu, R. Highly Specific and Sensitive Electrochemical Genotyping *via* Gap Ligation Reaction and Surface Hybridization Detection. *J. Am. Chem. Soc.* **2009,** *131*, 2478–2480.
23. Xiao, Y.; Pavlov, V.; Niazov, T.; Dishon, A.; Kotler, M.; Willner, I. Catalytic Beacons for the Detection of DNA and Telomerase Activity. *J. Am. Chem. Soc.* **2004,** *126*, 7430–7431.
24. Xue, X.; Xu, W.; Wang, F.; Liu, X. Multiplex Single-Nucleotide Polymorphism Typing by Nanoparticle-Coupled DNA-Templated Reactions. *J. Am. Chem. Soc.* **2009,** *131*, 11668–11669.
25. Liu, J.; Lu, Y. Preparation of Aptamer-Linked Gold Nanoparticle Purple Aggregates for Colorimetric Sensing of Analytes. *Nat. Protocols* **2006,** *1*, 246–252.
26. Liu, J.; Lu, Y. Fast Colorimetric Sensing of Adenosine and Cocaine Based on a General Sensor Design Involving Aptamers and Nanoparticles. *Angew. Chem., Int. Ed.* **2005,** *45*, 90–94.
27. Zhang, L.; Huang, C.; Li, Y.; Xiao, S.; Xie, J. Label-free Detection of Sequence-Specific DNA with Multiwalled Carbon Nanotubes and Their Light Scattering Signals. *J. Phys. Chem. B* **2008,** *112*, 7120–7122.
28. Song, Y.; Wang, X.; Zhao, C.; Qu, K.; Ren, J.; Qu, X. Label-free Colorimetric Detection of Single Nucleotide Polymorphism by Using Single-Walled Carbon Nanotube Intrinsic Peroxidase-like Activity. *Chem.—Eur. J.* **2010,** *16*, 3617–3621.
29. Deng, M.; Zhang, D.; Zhou, Y.; Zhou, X. Highly Effective Colorimetric and Visual Detection of Nucleic Acids Using an Asymmetrically Split Peroxidase DNAzyme. *J. Am. Chem. Soc.* **2008,** *130*, 13095–13102.
30. Li, T.; Dong, S.; Wang, E. Label-Free Colorimetric Detection of Aqueous Mercury Ion (Hg^{2+}) Using Hg2+-Modulated G-Quadruplex-Based DNAzymes. *Anal. Chem.* **2009,** *81*, 2144–2149.
31. He, S.; Song, B.; Li, D.; Zhu, C.; Qi, W.; Wen, Y.; Wang, L.; Song, S.; Fang, H.; Fan, C. A Graphene Nanoprobe for Rapid, Sensitive, and Multicolor Fluorescent DNA Analysis. *Adv. Funct. Mater.* **2010,** *20*, 453–459.

32. Lu, C.; Yang, H.; Zhu, C.; Chen, X.; Chen, G. A Graphene Platform for Sensing Biomolecules. *Angew. Chem., Int. Ed.* **2009,** *48*, 4785–4787.
33. Li, D.; Muller, M. B.; Gilje, S.; Kaner, R. B.; Wallace, G. G. *Nat.* Processable Aqueous Dispersions of Graphene Nanosheets. *Nanotechnol.* **2008,** *3*, 101–105.
34. Xu, Y. X.; Zhao, L.; Bai, H.; Hong, W. J.; Li, C.; Shi, G. Q. Chemically Converted Graphene Induced Molecular Flattening of 5,10,15,20-Tetrakis(1-methyl-4-pyridinio)porphyrin and Its Application for Optical Detection of Cadmium(II) Ions. *J. Am. Chem. Soc.* **2009,** *131*, 13490–13497.
35. Bianco, P.; Haladjian, J.; Draoui, K. Electrochemistry at a Pyrolytic Graphite Electrode: Study of the Adsorption of Hemin. *J. Electroanal. Chem.* **1990,** *279*, 305–314.
36. Su, Q.; Pang, S.; Alijani, V.; Li, C.; Feng, X.; Müllen, K. Composites of Graphene with Large Aromatic Molecules. *Adv. Mater.* **2009,** *21*, 3191–3195.
37. Graf, D.; Molitor, F.; Ensslin, K.; Stampfer, C.; Jungen, A.; Hierold, C.; Wirtz, L. Spatially Resolved Raman Spectroscopy of Single- and Few-Layer Graphene. *Nano Lett.* **2007,** *7*, 238–242.
38. Qutub, Y.; Uzunova, V.; Galkin, O.; Vekilov, P. G. Interactions of Hemin with Model Erythrocyte Membranes. *J. Phys. Chem. B* **2010,** *114*, 4529–4535.
39. Gao, L.; Zhuang, J.; Nie, L.; Zhang, J.; Zhang, Y.; Gu, N.; Wang, T.; Feng, J.; Yang, D.; Perrett, S.; Yan, X. Intrinsic Peroxidase-Like Activity of Ferromagnetic Nanoparticles Nature Nanotechnology. *Nat. Nanotechnol.* **2007,** *2*, 577–583.
40. Sano, M.; Okamura, J.; Shinkai, S. Colloidal Nature of Single-Walled Carbon Nanotubes in Electrolyte Solution: The Schulze−Hardy Rule. *Langmuir* **2001,** *17*, 7172–7173.
41. Hummers, W.; Offeman, R. J. Preparation of Graphitic Oxide. *J. Am. Chem. Soc.* **1958,** *80*, 1339–1339.
42. Guo, Y. J.; Guo, S. J.; Ren, J. T.; Zhai, Y. M.; Dong, S.; Wang, E. K. Cyclodextrin Functionalized Graphene Nanosheets with High Supramolecular Recognition Capability: Synthesis and Host−Guest Inclusion for Enhanced Electrochemical Performance. *ACS Nano* **2010,** *4*, 4001–4010.
43. Zhu, C. Z.; Guo, S. J.; Fang, Y. X.; Dong, S. J. Reducing Sugar: A Kind of New Functional Molecules for the Green Synthesis of Graphene Nanosheets. *ACS Nano* **2010,** *4*, 2429.